Elsevier Editorial System(tm) for Acta Materialia

Manuscript Draft

Manuscript Number:

Title: Achieving exceptional radiation tolerance with crystalline-amorphous nanocrystalline structure

Article Type: Full length article

Section/Category: No, do NOT opt in to First Look

Keywords: Nanocrystalline, amorphous intergranular film, radiation damage, molecular dynamics

Corresponding Author: Ms. Miaomiao Jin,

Corresponding Author's Institution: Massachusetts Institute of Technology

First Author: Miaomiao Jin

Order of Authors: Miaomiao Jin; Penghui Cao; Michael P Short

Abstract: Nanostructured materials with amorphous intergranular films (AIFs) have demonstrated superior strength and ductility. The radiation tolerance is expected to be high as the large fraction of interfacial volume efficiently sinks radiation-induced defects. Here, we demonstrate how a crystalline-amorphous system (nanocrystalline Cu with Zr doped AIFs) responds to continuous irradiation with molecular dynamics simulations. We propose a diffusion model that well characterizes the cascade-driven mixing process, and reveal that the spread of Zr distribution scales linearly with the damage level. The exceptional radiation resistance is attributed to that the interfaces are sustainable defect sinks, that Zr mixing into the bulk enhances local defect annihilation due to solute-interstitial dragging, and that Zr impedes radiation-enhanced grain growth by restraining AIFs from migration and maintaining interface stiffness. These findings suggest that AIF-engineered systems hold promise as highly radiation-tolerant materials with strong structural stability and self-healing capability under radiation damage.

Suggested Reviewers: Michael Demkowicz
Associate Professor, Materials Science & Engineering, Texas A&M University
demkowicz@tamu.edu
Prof. Demkowicz is one of the leading experts on computational materials design, especially radiation damage study of multi-layer materials, such as Cu-Nb.

Xianming Bai
Assistant Professor, Materials Science & Engineering, Virginia Tech
xmbai@vt.edu
Prof. Bai specializes in computational materials science with atomistic to mesoscale methods, and studying radiation effects in nuclear materials. He has published multiple renowned work on explaining material behavior driven by radiation.

Kai Nordlund
Professor, Physics, University of Helsinki
kai.nordlund@helsinki.fi
Prof. Nordlund is a leading expert on atomistic simulations of radiation and other non-equilibrium effects in all classes of materials. He has organized multiple conferences on radiation effects and defects in nanoscale materials.

Blas Uberuaga
Technical Staff Member, Materials Science and Technology Division, Los Alamos National Laboratory
blas@lanl.gov
Dr. Uberuaga is an expert in radiation damage study, and defect kinetics and evolution. He has published multiple very nice work on radiation effects and tolerance.

July 19, 2019

Dear Editor:

We would like to submit our manuscript entitled "Achieving exceptional radiation tolerance with crystalline-amorphous nanocrystalline structure" for publication in *Acta Materialia*.

The continued development of nuclear technologies for efficient utilization of nuclear power can meet the increasing demand for energy. However, structural materials in advanced nuclear systems suffer from high levels of radiation damage, making the design and development of radiation-tolerant materials of central importance. A new design based on interface engineering with amorphous intergranular films (AIFs) in nanocrystalline materials is attracting much attention due to its extraordinary properties.

In this work, for the first time, we use atomistic simulations to examine how a crystalline-amorphous system (nanocrystalline Cu with Zr-doped AIFs) responds to continuous irradiation. We demonstrate that these amorphous films not only act as effective sinks for radiation-induced defects, but also indicate strong thermal stability against radiation-enhanced grain growth and recrystallization. We also find that Zr atoms mixing into the grain interior can be well described by a multi-film diffusion model, and these mixed Zr atoms facilitate additional defect annihilation due to solute dragging effect.

The results provide atomistic details and quantitative analysis of radiation-induced system evolution and damage reduction mechanisms. More importantly, these findings suggest that AIF-engineered systems hold promise as highly radiation-tolerant materials with strong structural stability and self-healing capability under radiation damage.

Due to the importance of fundamental understanding and mechanistic explanation regarding the exceptional radiation tolerance in this material design, and due to the original insights that this work provides, we believe this work will have a significant impact on the fields of radiation science, materials science, and atomistic modeling and simulation. Therefore, we believe it to be appropriate for the scope & aims and wide readership of *Acta Materialia*.

Thank you for your consideration of our manuscript. For any questions or inquiries regarding our submission, please address Dr. Jin (the corresponding author) at mmjin@mit.edu.

Very sincerely,
Miaomiao Jin
Penghui Cao
Michael P. Short

-

# Achieving exceptional radiation tolerance with crystalline-amorphous nanocrystalline structure

Miaomiao Jin,[1,*] Penghui Cao,[2] and Michael P. Short[1]

[1] *Department of Nuclear Science and Engineering, Massachusetts Institute of Technology, 77 Massachusetts Ave, Cambridge, MA 02139, USA*

[2] *Department of Mechanical and Aerospace Engineering, University of California, Irvine, Irvine, CA 92697, USA*

## Abstract

Nanostructured materials with amorphous intergranular films (AIFs) have demonstrated superior strength and ductility. The radiation tolerance is expected to be high as the large fraction of interfacial volume efficiently sinks radiation-induced defects. Here, we demonstrate how a crystalline-amorphous system (nanocrystalline Cu with Zr-doped AIFs) responds to continuous irradiation with molecular dynamics simulations. We propose a diffusion model that well characterizes the cascade-driven mixing process, and reveal that the spread of Zr distribution scales linearly with the damage level. The exceptional radiation resistance is attributed to that the interfaces are sustainable defect sinks, that Zr mixing into the bulk enhances local defect annihilation due to solute-interstitial dragging, and that Zr impedes radiation-enhanced grain growth by restraining AIFs from migration and maintaining interface stiffness. These findings suggest that AIF-engineered systems hold promise as highly radiation-tolerant materials with strong structural stability and self-healing capability under radiation damage.

**Keywords:** Nanocrystalline, amorphous intergranular film, radiation damage, molecular dynamics

**Declarations of interest:** : none

* mmjin@mit.edu (Corresponding author)

## I. INTRODUCTION

Radiation-induced microstructural evolution accelerated by defects from atomic collisions can significantly modify the as-manufactured material properties, leading to phenomena such as grain growth, hardening, and swelling [1]. Hence, the capability to effectively control defect behavior is always emphasized in radiation resistant materials design. Nanostructured features in various forms such as nanocrystals, nanotwins, nanolaminates, and nanoparticles have received considerable interest due to numerous demonstrations of their potential to achieve exceptional radiation performance compared with conventional materials [2]. These nano-features share a common theme in promoting interface-mediated defect dynamics, in that the abundant interfaces provide ample sinks to defects.

Nanocrystalline (NC) materials are known to be radiation resistant compared to their coarse-grained counterparts [3, 4]. Samaras et al. proposed that the excess free volume granted by large grain boundary (GB) area can act as defect annihilation sites [5]. Later, Bai et al. [6] demonstrated that interstitials loaded into GBs can be emitted to annihilate nearby vacancies in grain interior. However, NC materials are known to experience rapid grain growth even at relatively low temperatures, due to the large driving force of grain coarsening facilitated by abundant GB areas. Such growth can be greatly enhanced by radiation [7–9] even when diffusion is very limited, which deteriorates the deliberate nanostructuring. Even worse, the combination of high temperature and intense radiation environment in future nuclear systems poses a grand challenge in the structural stability of NC materials.

The stability of NC materials can, nevertheless, be increased by kinetically pinning down boundary migration by Zener pinning [10] and solute drag [11], or thermodynamically reducing GB energy from tuning interfacial chemistry via dopant segregation [12, 13]. Kalidindi and Schuh introduced a stability criterion based on formation enthalpy difference between solutes segregating at GBs and solutes forming bulk phases [14]. In addition, entropy can also contribute to grain stabilization with reduced free energy [14, 15]. The resultant interfacial features known as complexions may be treated as a separate phase. Dillon et al. [16] theoretically predicted the existence of multiple types of interface complexions by thermodynamics, and suggested that mutual transformation can be achieved by chemistry and heat treatment to better control material properties. By combining complexion engineering and nanostructuring where each offers an edge on its own, the brittle issue of nanostructured

materials can be effectively alleviated. Both the ductility and toughness can be greatly improved by transforming GBs into amorphous intergranular films (AIFs), which breaks the common perception of strength-ductility trade-off [17, 18].

The structural stability and mechanical benefits of AIF-engineered interface complexions represent a viable stepping stone to radiation-tolerant material design. AIFs with large free volumes are expected to perform as well as, if not better than, GBs at ameliorating the accumulation of radiation damage. Based on the high glass-forming ability of Cu-Zr alloys [19], Ludy et al. built an atomistic Cu model with Zr-loaded GBs and showed that the AIF acts as an unbiased sink for both vacancies and interstitials [20], whereas GBs preferentially absorb the latter [4]. However, the evolution of the system during intense irradiation has yet to be determined. The uniqueness arises as the segregated atoms, which constitute the AIF, can migrate to the bulk region under the highly non-equilibrium condition, known as ion mixing. Although bilayer mixing has received considerable interest since 1970s for the purpose of materials modification [21–23], and a detailed description of the process as a function of irradiation dose has been given in [24], mixing behavior in this crystalline-amorphous system has not yet been characterized. Finally, the convolved evolution of defects and interfaces is of significant interest to evaluate material performance under irradiation. In this study, we use molecular dynamics (MD) and an algorithm to introduce consecutive damage cascades into a simulation cell to study the irradiation of an AIF system, with sufficient resolution to reveal the kinetics and mechanisms of its evolution. The Cu-Zr system is utilized as in the previous studies [18, 20], and its response to irradiation including ion-mixing behavior, defect dynamics, and interface stability is elaborated.

## II. METHODS AND MODELS

MD simulations with LAMMPS [25] are used to study the radiation damage process in a Zr-doped Cu bicrystal consisting of 235,200 atoms with a dimension 11.6 nm $\times$ 23.0 nm $\times$ 10.9 nm. Atomic interactions are described by an EAM potential from Borovikov et al. [26], which provides realistic stacking fault energies. The initial atomic configuration is prepared by referring to the procedure in previous Cu-Zr studies [18, 27]: i) a bicrystal with two high angle symmetric tilt $\Sigma5(210)$ GBs is created; ii) two slices of atoms containing the GBs are selected and 25% of Cu atoms are randomly replaced with Zr atoms; (iii) the two slices are

heated to 1600 K and held for 200 ps, while the rest atoms remain fixed; (iv) the two slices of atoms are quenched from 1600 K to 650 K over 200 ps; (v) the entire system is quenched from 650 K to 300 K over 200 ps; (vi) the system is relaxed at 300 K for 30 ps at zero pressure. This results in a configuration containing two AIFs. Figure 1 shows the structure and atom distribution, where atoms in the AIF are in short-range order, while sharp peaks in the crystalline part indicate long-range order. To characterize the effect of AIF thickness on its radiation performance, configurations with $d$ ranging from 1-5 nm are prepared.

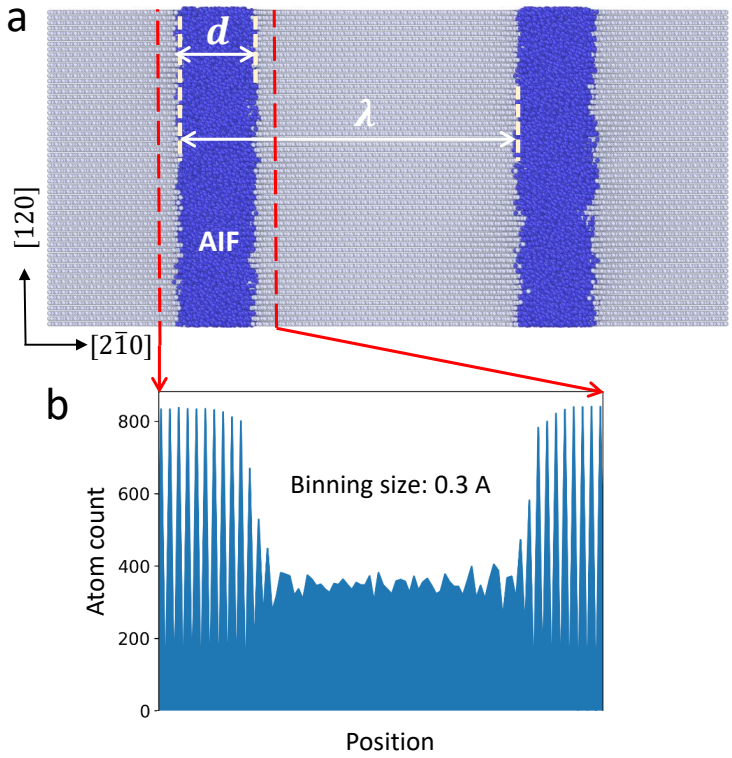


FIG. 1. (a) A bicrystal simulation cell containing two AIFs, which are constructed by heat treating $\Sigma5(210)$ GBs doped with Zr atoms (Cu-25 at.%Zr). $\lambda$ and $d$ denote AIF spacing and width, respectively. Atoms are colored by the structure type (gray: FCC (face centered cubic) atoms, blue: non-FCC atoms) (b) Atom distribution across the AIF region between the two red dashed lines, showing the crystalline and amorphous parts.

We follow the practice from [4] to simulate radiation damage due to overlapping cascades. The procedure is summarized here for the sake of completeness. Consecutive PKAs (primary knocked-on atoms) are randomly introduced into the initially configured simulation cell by assigning the selected atoms 5 keV kinetic energy with a random incident direction.

Periodic boundary conditions are applied along all three axes of the cell. To ensure that each damage cascade induced by the PKA is fully contained within the cell, atoms are shifted so that the PKA is always at the center before launching. To accommodate high energy collisions, the Ziegler-Biersack-Littmark (ZBL) repulsive potential [28] is smoothly joined to the aforementioned EAM potential [26]. Furthermore, an adaptive time-stepping technique is used to constrain the atomic movement to 0.05 Å per timestep. A thermal bath with a prescribed ambient temperature is created to simulate the environment and drain the excess energy. It is achieved by applying a temperature-rescaling thermostat to the atoms in the outermost layer of the simulation cell with a thickness of one lattice constant. After the system cools down, the cell is shifted back for consistent tracking of defect evolution. The system is adequately annealed to the ambient temperature in MD time frame ($\sim$ 30 ps) before launching another PKA. In the end, one can obtain $\sim$ 1 dpa according to Norgett-Robinson-Torrens (NRT) model, by increasing the number of PKAs as necessary. It should be noted that the simulated dose rate is orders of magnitude higher than that in experimental conditions. Nevertheless, this procedure allows one to probe the mechanisms underpinning defect-interface interaction, and examine defect dynamics in the temperature regimes where microstructural evolution is driven by damage cascades, rather than the long timescale thermal diffusion. System evolution is analyzed based on the atomic configurations, with representative ones available at [29]. Defects and defective structures are recognized by the Wigner-Seitz cell method [30] and common neighbor analysis [31] using the OVITO package [32].

## III. RESULTS

Transforming an interface from a GB to an AIF substantially changes its response to radiation. Figure 2 provides an overview of the two systems with increasing dose levels based on common neighbor analysis. Distinct contrast can be observed in both interface migration and defect morphologies. Here the GB is mobile and stacking fault tetrahedra (SFTs) frequently form in the GB system, whereas the AIF is immobile and fewer SFTs are produced in the AIF system. Since the behavior of NC Cu has been investigated in [4], the following sections elaborate on the behavior of the AIF system with frequent comparisons to GBs.

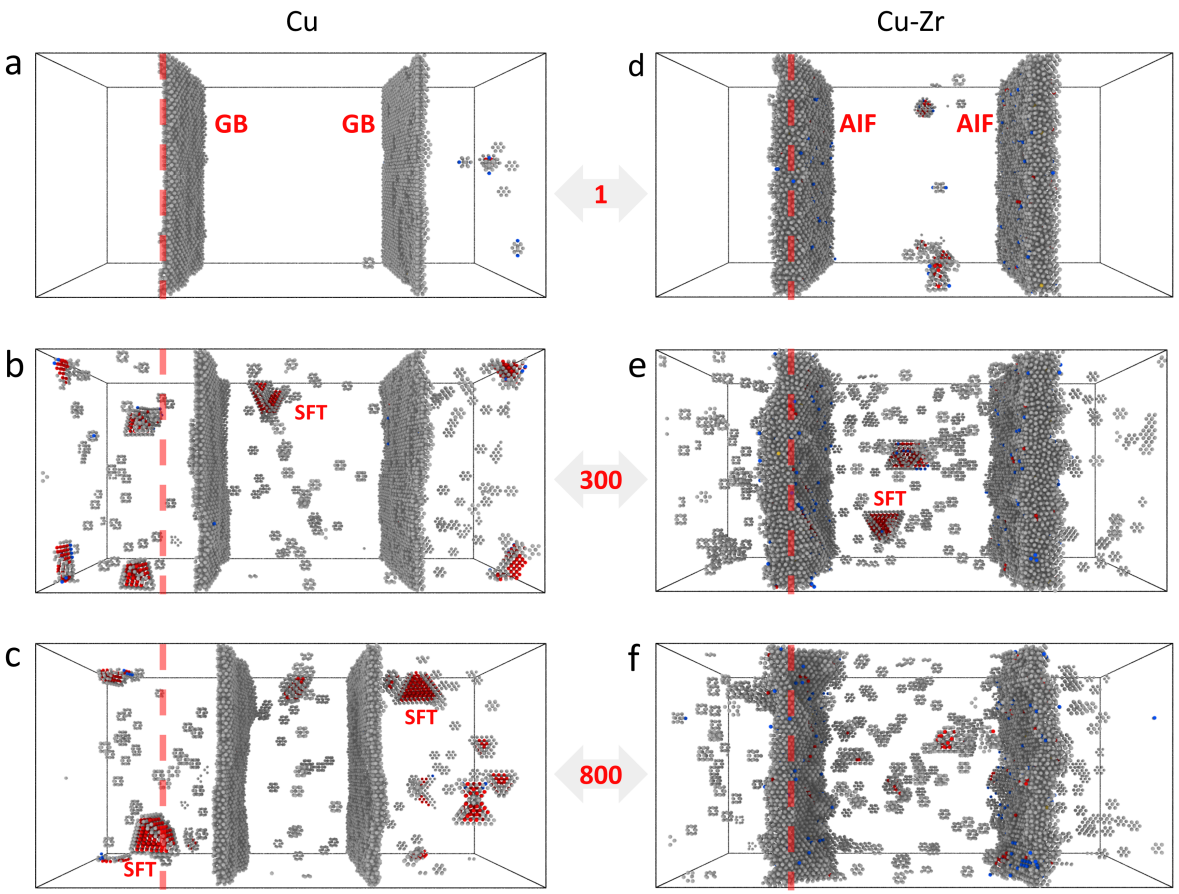


FIG. 2. Comparison of radiation response between bicrystal systems containing GBs (a-c) and AIFs (d-f). Non-FCC atoms are shown after 1, 300, and 800 damage cascades for each system at an ambient temperature of 800 K. The dashed red line marks the original position of the left interface. Multiple SFTs are recognized. The initial spacing between the interfaces is 11.6 nm and the AIF thickness is 12 Å. Grain stabilization and reduced defect cluster size have been observed in the AIF system. Atoms are colored by the structure type from common neighbor analysis (gray: unstructured atoms, red: hexagonal close packed atoms, blue: body centered cubic atoms, and FCC atoms are removed for clarity).

### A. Ion mixing

The displacement process which causes ion mixing is often described with two regimes: ballistic collision and thermal spike, where the latter involves multi-body interactions of particles within the cascade volume and redistributes the kinetic energy among a local pocket of atoms [33]. Previous theories have explained this mixing based on atom collision,

thermal spikes, and radiation-enhanced diffusion (RED) [24, 34]. It is expected that the majority of mixing takes place in thermal spike regime on the order of picoseconds, rather than the ballistic collision regime [33]. Using our multiple cascade MD scheme, the Zr atom distribution can be calculated at different dose levels to capture the kinetics of the ion mixing process. Considering the underlying connection to diffusion process during the thermal spike phase of a cascade [33], the distribution profile of Zr can be analogous to the solution of diffusion equation in a multi-film setting. Hence, the process is then characterized by curve fitting to the distribution suggested by the multi-film diffusion model. Consider a thin AlF layer sandwiched between two infinite bodies. The concentration of the solute $c(x,t)$ is described by the 1D diffusion equation,

$$\frac{\partial c(x,t)}{\partial t} = D\frac{\partial^2 c(x,t)}{\partial x^2} \tag{1}$$

where $D$ is the effective diffusivity of mixing, which ought to depend on material properties, temperature, and radiation parameters. The boundary and initial conditions are as follows,

$$c(\pm\infty, t) = 0 \tag{2}$$

$$c(x \leq -d/2, 0) = 0 \tag{3}$$

$$c(-d/2 < x < d/2) = c_0 \tag{4}$$

$$c(x \geq d/2, 0) = 0 \tag{5}$$

where $d$ is the thickness of the AlF layer centered at $x = 0$. The solution can be written as follows:

$$c(x,t) = \frac{c_0}{2}\left[\mathrm{erf}\left(\frac{x + d/2}{\sqrt{4Dt}}\right) - \mathrm{erf}\left(\frac{x - d/2}{\sqrt{4Dt}}\right)\right] \tag{6}$$

where erf is the error function and defined as,

$$\mathrm{erf}(x) \equiv \frac{2}{\sqrt{\pi}}\int_0^x e^{-t^2} dt \tag{7}$$

Note that due to the periodicity of AlFs in the configuration, the analytical solution $C(x,t)$ is a superposition of infinite single film solutions centered at locations separated by a spacing $\lambda$,

$$C(x,t) = \sum_{k=-\infty}^{+\infty} c(x + k\lambda, t) \tag{8}$$

As a simplification, three terms with centers at 0, $-\lambda$, and $\lambda$ (i.e. $k = 0, \pm 1$) are used to approximate the Zr distribution. Figure 3a schematically plots the evolution of this distribution. Initially, Zr atoms are concentrated inside the AIF (step function), then the profile starts to broaden due to mixing (red curve). With continued irradiation, the neighboring profiles start to overlap (blue curve). Using this model, Figure 3b demonstrates strong agreement between the calculated histograms and fitted curve, which indicates that the model is a good approximation of the simulated results.

The solute mixing profile is an accumulated consequence of temporal instantaneous atomic rearrangement ($\sim 10^{-11}s$) and spatially overlapping cascade volumes. The parameter $4Dt$ is an indicator to the distribution spread and ion mixing rate, hence, this quantity is retrieved at each dose level by fitting to the Zr distribution. Figure 4 shows that $4Dt$ scales linearly with dose $\phi$. Using $\beta$ to denote the slope from linear fitting, we have $4Dt = \beta\phi$. On one hand, AIF thickness does not exhibit obvious impact on $\beta$, which reinforces the assumption of the thin film diffusion model. This can be understood by recalling that the underlying atomic movement is dominated by liquid-like diffusion within the cascade volume. On the other hand, by increasing temperature, Zr atoms mix more efficiently during thermal spikes, and $\beta$ increases rapidly in the high temperature regime. It can be more clearly seen from the non-Arrhenius relation between $\ln\beta$ and $1/T$ shown in Figure 5. At high temperatures, RED which may lead to de-mixing is not accessible given the exceptionally high dose rate in MD simulations. Cu-Zr, nevertheless, has a negative heat of mixing [35], thus the mixed state could be metastable and resist de-mixing. Therefore, the depicted relation may still work at relatively high temperatures.

To delve deeper into the observed non-Arrhenius relation, the temperature effect is examined from the displacement of Zr atoms ($R^2_{Zr}$) across a cascade at various temperatures. To avoid the strong spatial dependence of Zr distribution, a randomly mixed Cu-Zr system is used. The mean squared displacement ($\widehat{R^2_{Zr}}$) after a cascade from a 5 keV recoil is then calculated with 50 samples. Figure 5 shows a strong linear relation between $\widehat{R^2_{Zr}}$ and $\beta$. Hence, given the dose rate and temperature, the cascade-driven mixing behavior reflects a random walk process, so $D \propto \beta \propto \widehat{R^2_{Zr}}$. It follows that $D$ has a non-Arrhenius relationship with $T$. The temperature variation stems from the characteristics of the cascade and internal chemical interactions. Figures 5c-d provide perspectives of the displacement field at 100 K and 800 K, demonstrating that i) the migration of Zr atoms is mainly confined to the ther-

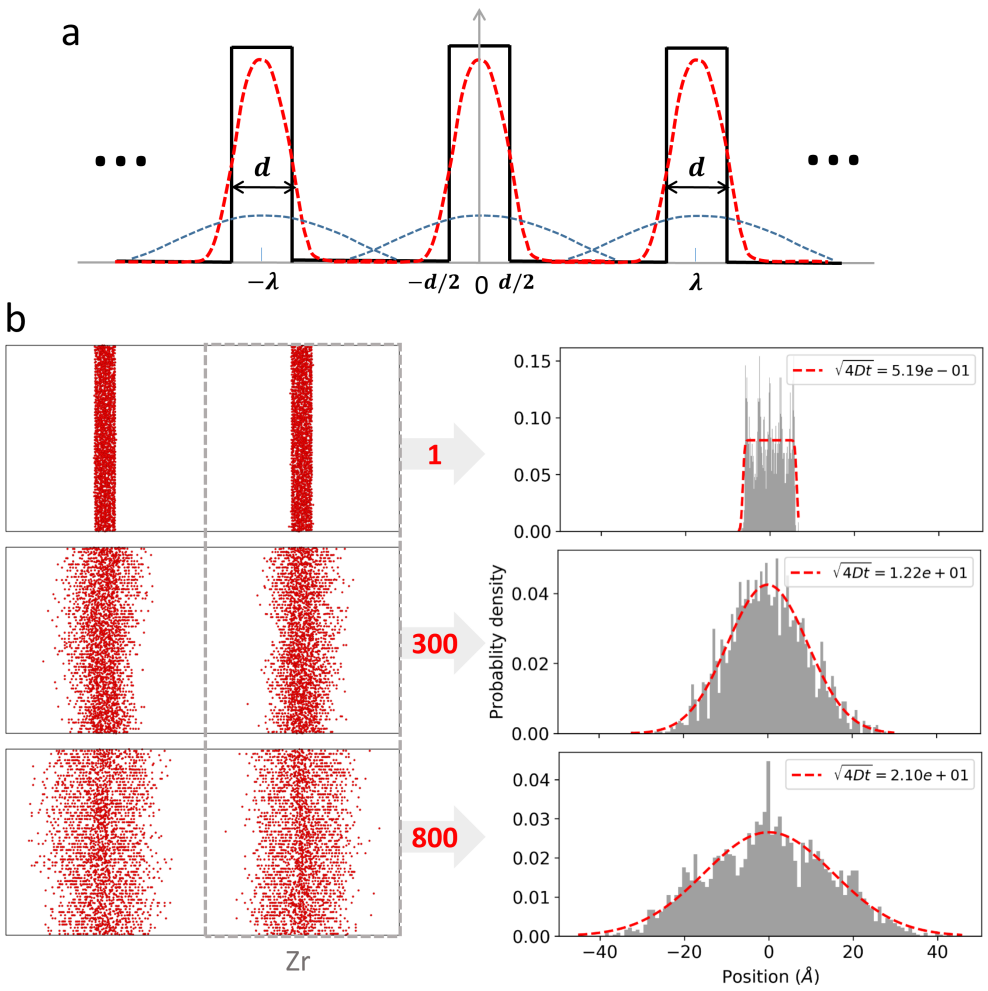


FIG. 3. (a) Schematic model and evolution of the concentration profile of Zr atoms in the AlF system with increasing dose. Starting with the initial condition (black curve) and before Zr atoms from neighboring AlFs coincide (red curve), the single film diffusion solution provides a good estimation of the Zr distribution. As overlap begins (blue curve), more terms must be incorporated to account for contributions from neighboring AlFs. (b) Left: Zr distribution in the simulation cell (red dots) on the same configurations in Figure 2(d-f); right: model fitting to the distribution (red dashed curve). $4Dt$ is a fitting parameter to the model.

mal spike volume at MD timescale, and ii) increasing ambient temperature induces larger cascade volume and $R^2_{Zr}$. The chemical interaction can be taken into account by modifying the atomic diffusion coefficient with the so-called Darken biasing factor $(1 - \frac{2\Delta H_{mix}}{k_b T})$ [33, 34], where $\Delta H_{mix}$ is the heat of mixing. However, by calculation, chemical interaction alone can not explain the non-Arrhenius relationship between $D$ and $T$. As suggested by Vineyard's

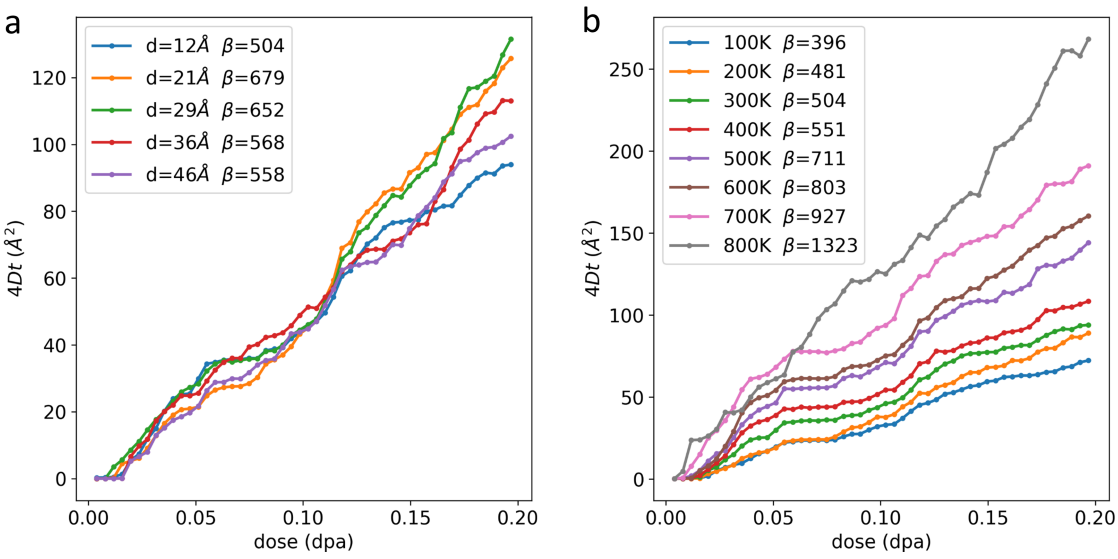


FIG. 4. (a) Fitting parameter $4Dt$ of the Zr concentration profile with respect to dose for systems with different AlF thickness $d$. (b) $4Dt$ with respect to dose for systems with $d = 12$ Å and different ambient temperatures. $\beta$ denotes the slope of the linear regression.

model on calculating activated events during thermal spikes [36], the temperature dependence of local heat capacity and thermal conductivity, which dictates how effectively the kinetic energy is transported away to the surrounding matter, may theoretically explain the relation.

### B. Defect reduction

The ample amount of interfacial volume provide efficient sinks for defects. With dopant atoms and subsequent ion mixing, unique features emerge in defect reduction mechanisms. Since interstitials are usually much more mobile than vacancies, they predominately migrate to sinks. In comparison, vacancies are mostly left in the bulk, mainly in the form of isolated point defects and SFTs. A detailed examination reveals that the pattern of SFTs in the bulk region evolves with the level of ion mixing, as schematically depicted in Figure 6 (see supplementary video for complete system evolution). At low dose before many Zr atoms migrate to the bulk, large SFTs form due to vacancy aggregation and direct production from damage cascades (stage I). At intermediate dose, the dispersion of Zr atoms shrinks the pristine Cu region, which decreases both the number of SFTs and their size (stage II).

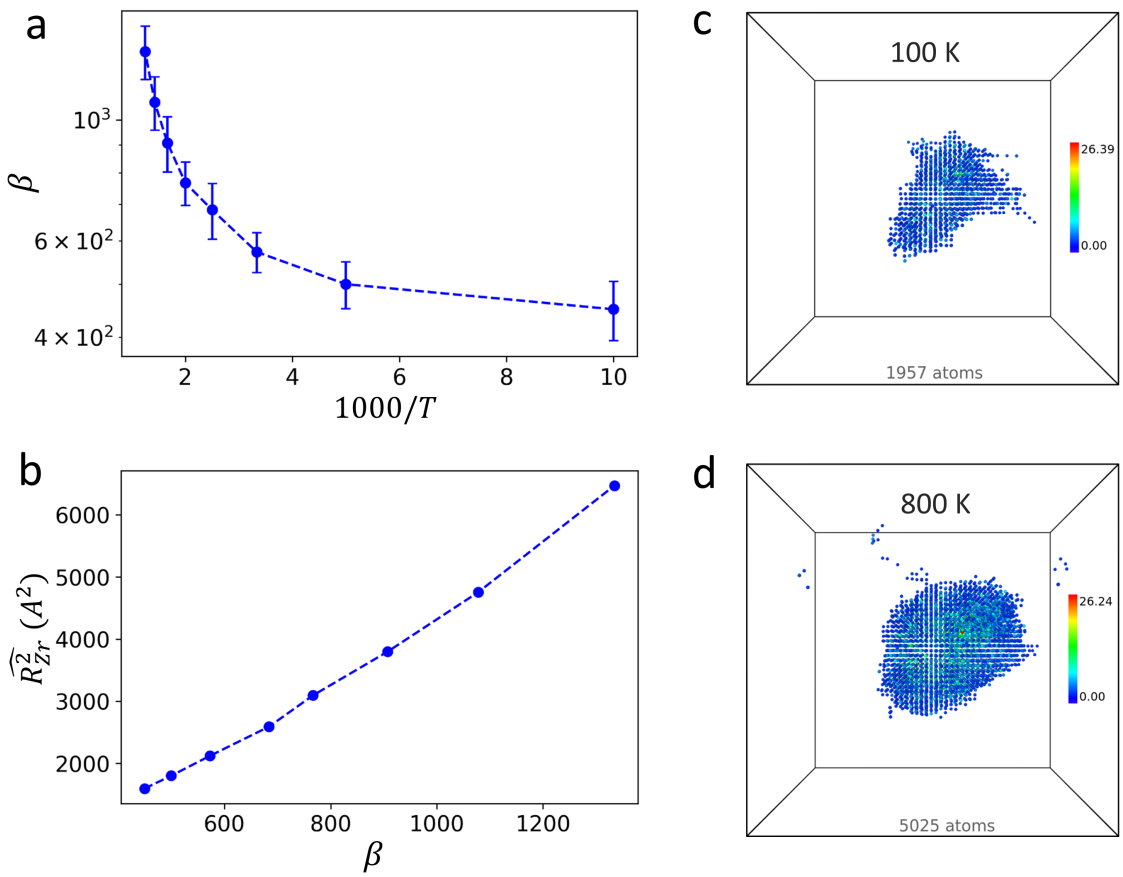


FIG. 5. (a) $\beta$ with respect to temperature. Each point is obtained from statistics of 10 calculations. The AIF thickness is 12 Å. (b) Linear correlation between $\widehat{R^2_{Zr}}$ and $\beta$. $\widehat{R^2_{Zr}}$ is an average of 50 calculations of Zr atom squared displacement after a cascade, with system dimension 11 nm x 11 nm x 11 nm and 4.65 at.% Zr. Using the same system, (c-d) shows a snapshot of atoms with a displacement larger than 2.55 Å at 100 K and 800 K after a cascade, where the latter induces a larger cascade volume involving migration of more atoms. Atoms are colored by the magnitude of their displacement.

Finally, as Zr distributions start to overlap from neighboring AIFs, only small and infrequent SFTs are observed (stage III). This evolution is directed by solutes which can influence the direct defect production from cascades and slow down defect diffusion due to defect-solute binding [1]. The binding energies between Cu point defects and Zr atoms at lattice sites are calculated with molecular statics using the same interatomic potential: $E_b$(vacancy, Zr)=0.11 eV and $E_b$([100] dumbbell, Zr)=0.36 eV. Such temporary trapping of defects near solute atoms, especially interstitials, increases the chance of vacancy annihilation rather

than forming large SFTs.

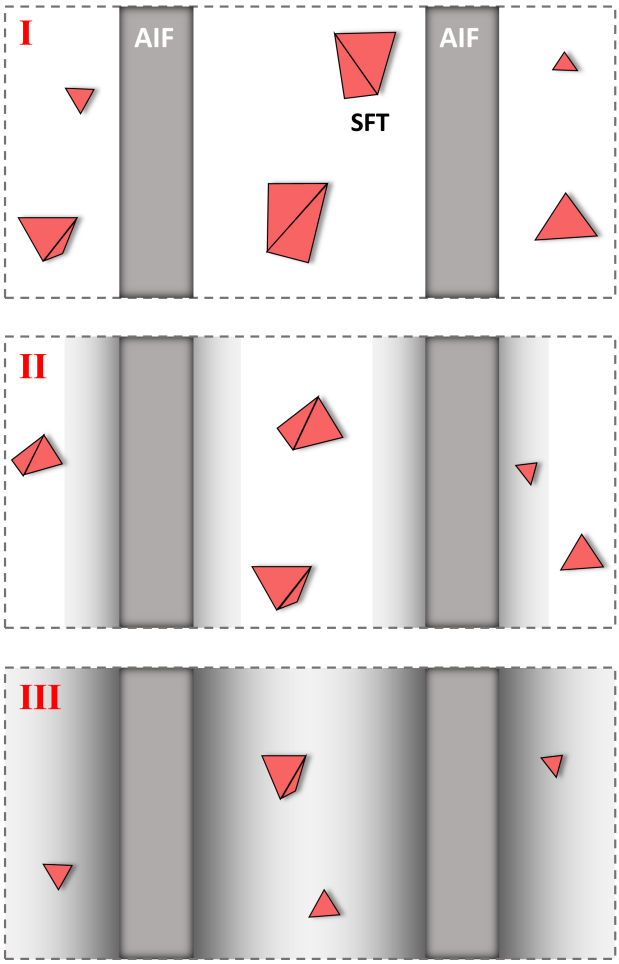


FIG. 6. Morphology of defect clusters (SFTs, red) with ion mixing level. The shade schematically indicates the Zr concentration in the bulk region. Stage I: before mixing or slight mixing, large SFTs form due to vacancy aggregation and direct production from damage cascades. Stage II: intermediate mixing, the dispersion of Zr atoms shrinks the pristine Cu region, which decreases both the number of SFTs and their size. Stage III: high mixing, only small and infrequent SFTs are observed.

To analyze the efficiency of damage reduction, the defect cluster size distribution and number density of defects are quantified and compared with GB system. It is worth mentioning that the Zr atoms on Cu lattice sites are not treated as defects during our analysis, and it is found that the mixed Zr atoms mainly reside at lattice points rather than interstitial sites. Figure 7a plots the accumulated size distribution of bulk defective structures based on non-FCC atoms across 500 cascades at 800 K (ambient temperature). The comparison

between the "Cu-Zr-AIF" and "Gu-GB" systems quantitatively demonstrates that the AIF system much better resists the creation of large defects. The number densities of point defects in the bulk region of the two systems are depicted in Figure 7b. The defects are vacancy-type dominated for both systems, but the AIF system appears to outperform the GB one by saturating at a lower defect density. Although both systems excel at restoring crystal structure by removing radiation-induced defects, there is a key difference in mechanisms beside that the interfaces are efficient sinks. In "Cu-GB," large mobile SFTs frequently form, and they can migrate to GBs and be absorbed [4]. However, in "Cu-Zr-AIF," mixing of Zr atoms facilitates local recombination of defects in the bulk due to defect-solute binding. Therefore, ion mixing can be a critical contributing factor to the damage reduction of an AIF-engineered system.

### C. Interface evolution

The solute atoms can not only kinetically pin down the interface from migration, but also thermodynamically decrease interfacial energy to slow down grain growth. Therefore, although radiation drives the system highly out of equilibrium, it is expected that the mobility of AIF decreases significantly compared with GB. Figure 8 monitors the interface position for "Cu-Zr-AIF" and "Gu-GB" systems during the same radiation conditions. The position is calculated by averaging the horizontal coordinates of all the constitutive atoms of the interfaces. Under the random disturbance of cascades, in the "Cu-Zr-AIF" system both AIFs barely move, while in "Gu-GB" system the GBs approach each other, indicating grain growth. It is promising that the application of AIF-engineered materials in nuclear systems can significantly alleviate the concern of grain growth and associated mechanical degradation.

The typical morphology of the interfaces during simulations is visualized in Figure 9 for both systems. Due to the pinning provided by Zr atoms, AIFs are stiff throughout radiation while irradiated GBs can be easily distorted due to interaction with large SFTs [4]. This stiffness leads to little curvature, and also accounts for the resistance from migration. The structure of AIFs is stable with occasional local reduction in thickness (Figure 9a). This fluctuation comes from direct bombardment of PKAs and local atomic rearrangement. No apparent recrystallization was observed. It is not yet clear whether the continuous draining

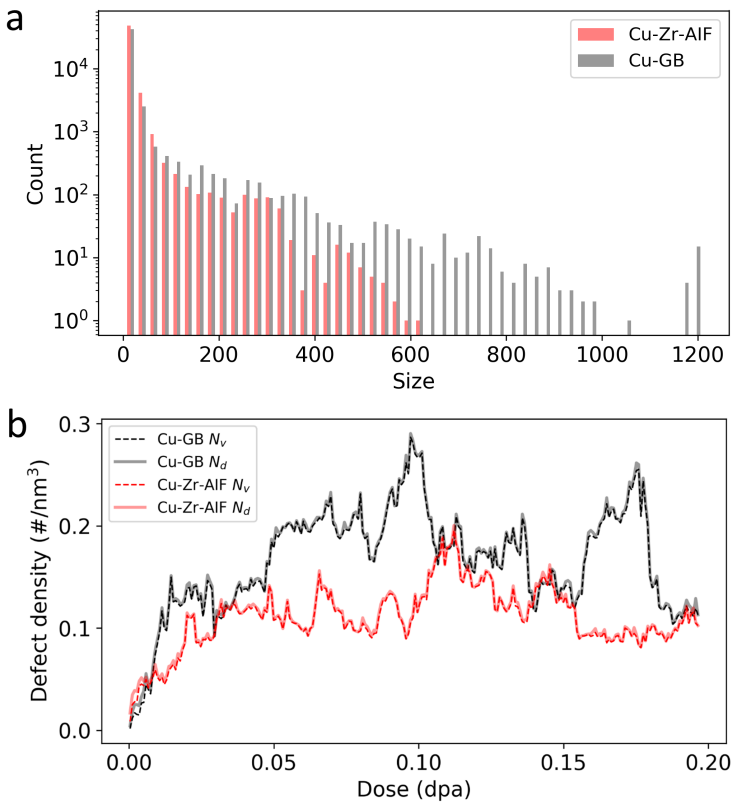


FIG. 7. (a) Size distribution of accumulated defective structures based on non-FCC atoms from common neighbor analysis during 1-500 cascade incidents in "Cu-Zr-AIF" (red) and "Gu-GB" (gray) systems. (b) Vacancy ($N_v$, dashed curve) and total defect ($N_d$, solid curve) density in the bulk region of "Cu-Zr-AIF" (red) and "Gu-GB" (gray) systems with increasing damage level. Total number of defects include both vacancies and interstitials. System settings: $\lambda = 11.6\,\text{nm}$, ambient temperature 800 K, and thickness of AIF 12 Å.

of Zr atoms from AIFs will lead to recrystallization, which can be an interplay between temperature, dose rate, mixing, and de-mixing trends.

## IV. DISCUSSION

The exceptional radiation performance of the AIF system complements the previously established strong mechanical properties. Compared with conventional interface engineering via GB, construction of AIFs by segregating glass-forming solutes introduces additional complexity in modeling and simulations. Since MD has minimal empirical parameters besides a prescribed potential, it offers a high fidelity picture of the mechanisms and kinetics

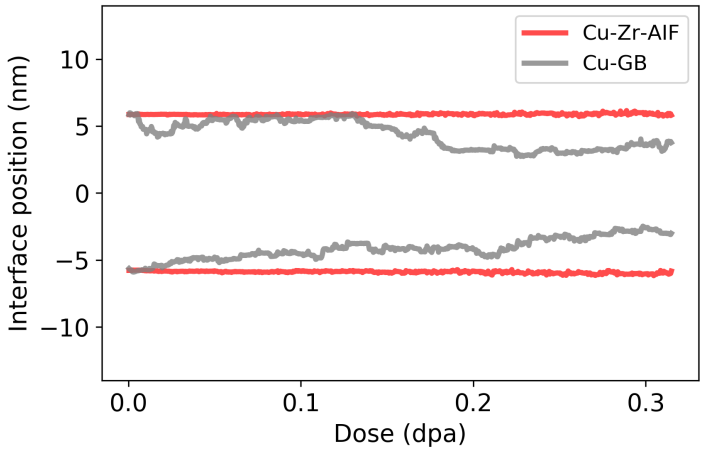


FIG. 8. Interface position in "Cu-Zr-AIF" (red) and "Gu-GB" (gray) systems with increasing damage level. System settings: $\lambda = 11.6\,\text{nm}$, ambient temperature 800 K, and thickness of AIF 12 Å.

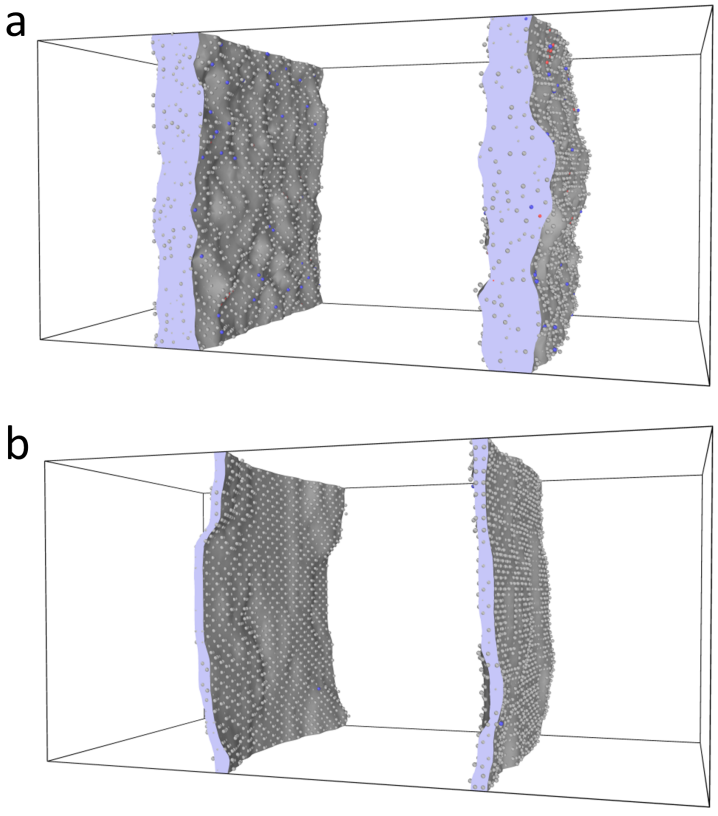


FIG. 9. Typical interface morphology in "Cu-Zr-AIF" (a) and "Gu-GB" (b) systems during irradiation. AIFs appear stiff due to solute pinning while GBs are more flexible.

of radiation assisted system evolution. The inevitable high dose rate in MD suggests that current results most readily apply to low temperature irradiation or damage cascade dominated processes. Extrapolation beyond these conditions needs further evaluation of thermal diffusion on much longer timescale beyond MD, using methods such as kinetic Monte Carlo and rate theory [1].

The as-prepared system concentrates the solute atoms within AIFs, and the consecutive incident ions drive the mixing of solutes in the bulk. No stoichiometric compound formation is favorable in this Cu-Zr system, hence the cascade-driven mixing behavior is characterized by the random walk process or diffusion model. In the current AIF configuration, direct statistics of the Zr distribution are well described by a superposition of multiple single thin-film diffusion solutions. The fitting parameter $4Dt$ as an indicator of the distribution spread, scales linearly with dose, which is consistent with previous experiments on ion mixing in bilayers using heavy ion bombardment [33]. The slope $\beta$ is independent of AIF thickness, but dependent on the ambient temperature. By the shape of $\beta$ and $1/T$, there appears a critical temperature around 200 K, below which $Dt$ is approximately independent of temperature and above which it increases rapidly. Such temperature dependence only comes from the characteristics of damage cascades, where high temperatures induce larger thermal spike volume accommodating more efficient Zr mixing.

Previous studies have discussed in detail the mixing in bilayer systems with experiments and theories [21–24, 34]. At low temperatures where RED is suppressed, based on the thermal spike model, the degree of mixing in bilayers was described as,

$$4Dt \propto \frac{1}{\Delta H_{coh}^2}(1 + K\frac{\Delta H_{mix}}{\Delta H_{coh}}) \tag{9}$$

where $\Delta H_{coh}$ is the cohesive energy and $K$ is a constant [33], and the correlation was later validated with experiments on metallic layers under low temperature irradiation [22]. As an alternate to the bilayer structure, ion mixing in these sandwiched AIFs may depend on thermodynamic properties with a similar formulation. Further work is needed to verify this hypothesis by studying multiple combinations of elements in stable AIF systems. Some possibilities include both positive (e.g. Cu-Nb, Ag-Mo) and negative (e.g. Ni-Zr and Ni-Nb) heat of mixing [35]. At high temperatures, it was proposed that RED beyond the cascade region contributes to increased or decreased mixing [34, 37]. Despite longer time scale RED being inaccessible in this study, the temperature dependence of the mixing still

resembles experimental results [21]. It implies that cascade-driven atom mixing can still be the main factor in high temperature scenarios. Additional simulations show that if we continue introducing cascades into the system, Zr atoms eventually become well-mixed with Cu atoms, consistent with the model prediction. The system can be metastable. Although there is a thermodynamic driving force for Zr to segregate to GBs as shown in [17], it is unclear whether segregation is still preferable with constructed AIFs. If de-mixing were to be favored, which has not been observed in the simulations, mixing would be much slower due to potential de-mixing at realistic dose rates and a high temperature irradiation environment. Moreover, this study considers low energy recoil events with 5 keV PKAs, where mixing during the thermal spikes is dominant compared with initial ballistic mixing. However, high energy recoils may contribute to the long range relocation of atoms [21], which can change the mixing behavior and its temperature dependence.

The damage reduction capability is quantified through the defect number density and size distribution. By launching a close-by PKA towards the AIF, Ludy et al. [20] found that these amorphous films are unbiased sinks to both vacancies and interstitials. This may reflect an intrinsic property of AIFs, however, the overall efficacy of AIFs in removing defects depends on the defect properties and dynamics in the bulk. The volume ratio of AIFs to bulk remains small such that direct interaction between an AIF and a cascade is not representative enough to describe spatially random cascade events. In fact, most cascades do not directly interact with AIFs, and the residual defects from these cascades in the bulk attempt to diffuse away. Interstitials with a high mobility are preferentially absorbed by AIFs, with more vacancies left behind. For those cascades that overlap with AIFs, unbiased ultra-efficient defect absorption can be expected. Additional defect control comes from ion mixing. Zr atoms mixed in the bulk can create a heterogeneous potential energy landscape due to chemical interaction and lattice mismatch [38]. Not only does defect migration become more heterogeneous which leads to limited long-range 1D diffusion, but also the solute dragging increases the chance of vacancy-interstitial recombination by slowing down interstitial migration [1]. This has at least three implications: i) interstitials are less likely to escape the cascade region in the presence of Zr atoms, suppressing the direct production of larger vacancy clusters; ii) interstitials are more likely to recombine with vacancies in the bulk; iii) vacancies are less likely to aggregate into large SFTs due to increased chance of recombination. The observations of decreasing SFT size with increasing degree of Zr

mixing corroborates the description. Compared with the GB system, AIFs demonstrate better performance in maintaining low defect density and small defect cluster size.

Grain growth in NC materials can be greatly accelerated by radiation [39]. A power law relationship between average grain size and irradiation dose was established with an exponent dependent on various factors such as microstructure and temperature [40]. Kaoumi et al. [8] proposed a theoretical analysis based on the direct impact of the thermal spikes on GBs and obtained an experimentally consistent exponent equal to 3. In comparison, the migration of interfaces significantly slows down in the AIF system, as the solute atoms effectively pin down their motion. The inertia of these interfaces during radiation signifies that radiation-enhanced grain growth can be significantly reduced. It remains to be confirmed whether the power law also applies to this system with a much smaller exponent. Experiments are more adaptable to resolve this question first, as complexity in theoretical treatment quickly builds up because of the chemical interactions, solute pinning, and ion mixing. Throughout the radiation process, the integrity of AIFs is maintained, i.e. the deficiency of Zr atoms does not alter the amorphous nature of the interfaces. It may be valid for low temperature radiation, but this raises a question about whether recrystallization occurs as Zr migrates away from AIFs with a low dose rate, high temperature environment. Furthermore, AIFs show high stiffness and minor morphological distortion. Such a lack of curvature leads to little driving force of migration, as opposed to the GB system where curved boundaries can allows a migration velocity three orders of magnitude higher than that of a planar boundary [9].

## V. CONCLUSION

We have demonstrated that AIFs function as more radiation-resistant interfaces in nanocrystalline (NC) materials compared to grain boundaries. The specific AIFs are created by transforming GBs into AIFs with Zr doping in NC Cu system. The response to continuous irradiation using MD simulations is elaborated. These amorphous films not only act as effective defect sinks, but also indicate strong thermal stability against radiation-enhanced grain growth and recrystallization. Upon irradiation, Zr atoms mix into the bulk by cascade-driven mixing process, which can be well described by a multi-film diffusion model. These mixed atoms facilitate more efficient defect annihilation due to solute

dragging effect. Although Cu-Zr system is the focus of study here, from the mechanistic perspective, it is expected that other combinations of elements with a high glass-forming capability would demonstrate similar behavior under irradiation. Hence, using AIFs may prove useful as a material design principle to develop highly radiation tolerant structural materials for nuclear applications. Further work on experimental verification is needed, especially the mixing/de-mixing behavior, the grain growth rate of the system, and stability of AIFs under different radiation conditions.

## ACKNOWLEDGMENT

The authors acknowledge support by the Idaho National Laboratory (INL) Nuclear University Consortium (NUC) under the Laboratory Directed Research and Development Grant No. 10-112583, by the U.S. Department of Energy NEUP Grant DE-NE0008450, and by the National Science Foundation CAREER Grant DMR-1654548.

[1] G. S. Was. *Fundamentals of radiation materials science: metals and alloys*. Springer, 2016.

[2] X. Zhang, K. Hattar, Y. Chen, L. Shao, J. Li, C. Sun, K. Yu, N. Li, M. L. Taheri, H. Wang, J. Wang, and M. Nastasi. Radiation damage in nanostructured materials. *Progress in Materials Science*, 96:217–321, 2018.

[3] C. Du, S. Jin, Y. Fang, J. Li, S. Hu, T. Yang, Y. Zhang, J. Huang, G. Sha, Y. Wang, Z. Shang, X. Zhang, B. Sun, S. Xin, and T. Shen. Ultrastrong nanocrystalline steel with exceptional thermal stability and radiation tolerance. *Nature Communications*, 9(1):5389, 2018.

[4] M. Jin, P. Cao, S. Yip, and M. P. Short. Radiation damage reduction by grain-boundary biased defect migration in nanocrystalline Cu. *Acta Materialia*, 155:410–417, 2018.

[5] M. Samaras, P. Derlet, H. Van Swygenhoven, and M. Victoria. Atomic scale modelling of the primary damage state of irradiated fcc and bcc nanocrystalline metals. *Journal of Nuclear Materials*, 351(1):47–55, 2006.

[6] X. Bai, A. F. Voter, R. G. Hoagland, M. Nastasi, and B. P. Uberuaga. Efficient annealing of radiation damage near grain boundaries via interstitial emission. *Science*, 327(5973):1631–1634, 2010.

[7] D. Bufford, F. Abdeljawad, S. Foiles, and K. Hattar. Unraveling irradiation induced grain growth with in situ transmission electron microscopy and coordinated modeling. *Applied Physics Letters*, 107(19):191901, 2015.

[8] D. Kaoumi, A. Motta, and R. Birtcher. A thermal spike model of grain growth under irradiation. *Journal of Applied Physics*, 104(7):073525, 2008.

[9] M. Jin, P. Cao, and M. P. Short. Mechanisms of grain boundary migration and growth in nanocrystalline metals under irradiation. *Scripta Materialia*, 163:66–70, 2019.

[10] J. Gao, R. G. Thompson, and B. R. Patterson. Computer simulation of grain growth with second phase particle pinning. *Acta Materialia*, 45(9):3653–3658, 1997.

[11] A. Michels, C. Krill, H. Ehrhardt, R. Birringer, and D. Wu. Modelling the influence of grain-size-dependent solute drag on the kinetics of grain growth in nanocrystalline materials. *Acta Materialia*, 47(7):2143–2152, 1999.

[12] Y. Zhang, G. J. Tucker, and J. R. Trelewicz. Stress-assisted grain growth in nanocrystalline metals: Grain boundary mediated mechanisms and stabilization through alloying. *Acta Materialia*, 131:39–47, 2017.

[13] R. Kirchheim. Grain coarsening inhibited by solute segregation. *Acta Materialia*, 50(2):413–419, 2002.

[14] A. R. Kalidindi and C. A. Schuh. Stability criteria for nanocrystalline alloys. *Acta Materialia*, 132:128–137, 2017.

[15] N. Zhou, T. Hu, J. Huang, and J. Luo. Stabilization of nanocrystalline alloys at high temperatures via utilizing high-entropy grain boundary complexions. *Scripta Materialia*, 124:160–163, 2016.

[16] S. J. Dillon, M. Tang, W. C. Carter, and M. P. Harmer. Complexion: a new concept for kinetic engineering in materials science. *Acta Materialia*, 55(18):6208–6218, 2007.

[17] A. Khalajhedayati, Z. Pan, and T. J. Rupert. Manipulating the interfacial structure of nanomaterials to achieve a unique combination of strength and ductility. *Nature Communications*, 7:10802, 2016.

[18] Y. Wang, J. Li, A. V. Hamza, and T. W. Barbee. Ductile crystalline–amorphous nanolaminates. *Proceedings of the National Academy of Sciences*, 104(27):11155–11160, 2007.

[19] D. Wang, Y. Li, B. Sun, M. Sui, K. Lu, and E. Ma. Bulk metallic glass formation in the binary Cu–Zr system. *Applied Physics Letters*, 84(20):4029–4031, 2004.

[20] J. E. Ludy and T. J. Rupert. Amorphous intergranular films act as ultra-efficient point defect sinks during collision cascades. *Scripta Materialia*, 110:37–40, 2016.

[21] F. Besenbacher, J. Bøttiger, S. Nielsen, and H. J. Whitlow. Short- and long-range ion-beam mixing in Cu: Al. *Applied Physics A*, 29(3):141–145, 1982.

[22] T. Workman, Y. Cheng, W. Johnson, and M.-A. Nicolet. Effect of thermodynamics on ion mixing. *Applied Physics Letters*, 50(21):1485–1487, 1987.

[23] M. Van Rossum, Y.-T. Cheng, M.-A. Nicolet, and W. Johnson. Correlation between cohesive energy and mixing rate in ion mixing of metallic bilayers. *Applied Physics Letters*, 46(6):610–612, 1985.

[24] P. Sigmund and A. Gras-Marti. Theoretical aspects of atomic mixing by ion beams. *Nuclear Instruments and Methods*, 182:25–41, 1981.

[25] S. Plimpton, P. Crozier, and A. Thompson. Lammps-large-scale atomic/molecular massively parallel simulator. *J. Comp. Phys.*, 18, 2007.

[26] V. Borovikov, M. I. Mendelev, and A. H. King. Effects of stable and unstable stacking fault energy on dislocation nucleation in nano-crystalline metals. *Modelling and Simulation in Materials Science and Engineering*, 24(8):085017, 2016.

[27] Z. Pan and T. J. Rupert. Amorphous intergranular films as toughening structural features. *Acta Materialia*, 89:205–214, 2015.

[28] J. F. Ziegler, J. P. Biersack, and U. Littmark. *The Stopping and Range of Ions in Solids*. Pergamon Press, 1985.

[29] M. Jin, P. Cao, and M. Short. Data repository supporting this manuscript, available at https://doi.org/10.5281/zenodo.3342916, 2019.

[30] K. Nordlund, M. Ghaly, R. Averback, M. Caturla, T. D. de La Rubia, and J. Tarus. Defect production in collision cascades in elemental semiconductors and fcc metals. *Physics Review B*, 57(13):7556, 1998.

[31] A. Stukowski. Structure identification methods for atomistic simulations of crystalline materials. *Modelling and Simulation in Materials Science and Engineering*, 20(4):045021, 2012.

[32] A. Stukowski. Visualization and analysis of atomistic simulation data with ovito–the open visualization tool. *Modelling and Simulation in Materials Science and Engineering*, 18(1):015012, 2009.

[33] W. Johnson, Y. Cheng, M. Van Rossum, and M. Nicolet. When is thermodynamics relevant to ion-induced atomic rearrangements in metals? *Nuclear Instruments and Methods in Physics Research Section B: Beam Interactions with Materials and Atoms*, 7:657–665, 1985.

[34] R. Averback. Fundamental aspects of ion beam mixing. *Nuclear Instruments and Methods in Physics Research Section B: Beam Interactions with Materials and Atoms*, 15(1-6):675–687, 1986.

[35] B. Liu, W. Lai, and Q. Zhang. Irradiation induced amorphization in metallic multilayers and calculation of glass-forming ability from atomistic potential in the binary metal systems. *Materials Science and Engineering: R: Reports*, 29(1-2):1–48, 2000.

[36] G. Vineyard. Thermal spikes and activated processes. *Radiation effects*, 29(4):245–248, 1976.

[37] B. Paine and R. S. Averback. Ion beam mixing: basic experiments. *Nuclear Instruments and Methods in Physics Research Section B: Beam Interactions with Materials and Atoms*, 7:666–675, 1985.

[38] M. Jin, P. Cao, and M. P. Short. Thermodynamic mixing energy and heterogeneous diffusion uncover the mechanisms of radiation damage reduction in single-phase Ni-Fe alloys. *Acta Materialia*, 147:16–23, 2018.

[39] H. A. Atwater, C. V. Thompson, and H. I. Smith. Ion-bombardment-enhanced grain growth in germanium, silicon, and gold thin films. *Journal of Applied Physics*, 64(5):2337–2353, 1988.

[40] J. C. Liu, M. Nastasi, and J. Mayer. Ion irradiation induced grain growth in Pd polycrystalline thin films. *Journal of Applied Physics*, 62(2):423–428, 1987.

**Radiation-induced evolution for CuZr-AIF system at 800K**

**Click here to download Supplementary Material: CuZr_AIF_800K_defective_structures.mp4**

**Radiation-induced evolution for Cu-GB system at 800K**

**Click here to download Supplementary Material: Cu_210GB_800K_defective_structures.mp4**

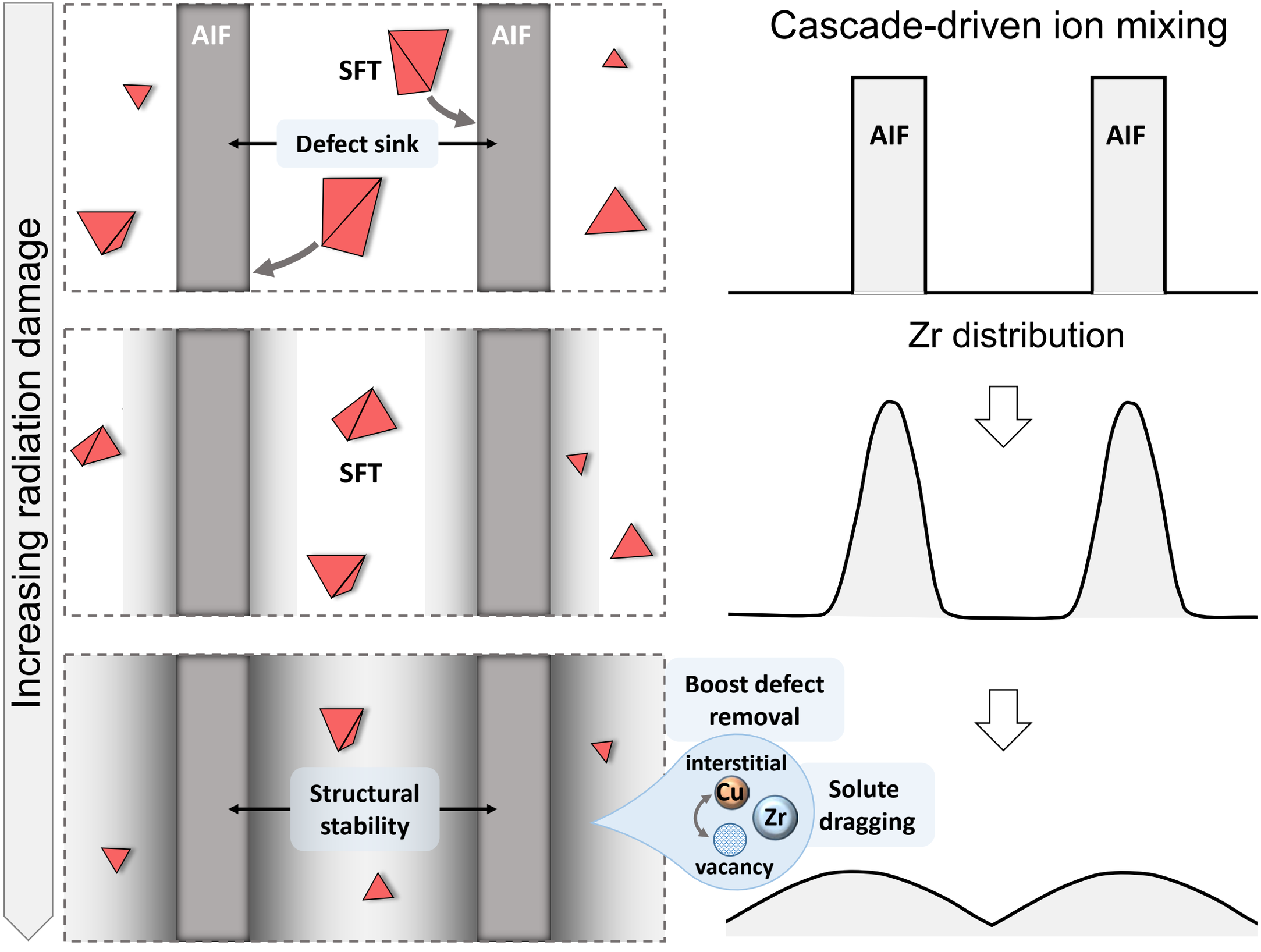
Increasing radiation damage
AIF
AIF
SFT
Defect sink
SFT
Structural stability
Boost defect removal
interstitial
Cu
Zr
vacancy
Solute dragging
Cascade-driven ion mixing
AIF
AIF
Zr distribution